A Two-Season Impact Study of Satellite and In Situ Data in the NCEP Global Data Assimilation System

TOM H. ZAPOTOCNY

Cooperative Institute for Meteorological Satellite Studies, and Space Science and Engineering Center, University of Wisconsin— Madison, Madison, Wisconsin, and Joint Center for Satellite Data Assimilation, Camp Springs, Maryland

JAMES A. JUNG

Cooperative Institute for Meteorological Satellite Studies, University of Wisconsin—Madison, Madison, Wisconsin, and Joint Center for Satellite Data Assimilation, Camp Springs, Maryland

JOHN F. LE MARSHALL

University of Maryland, College Park, College Park, and Joint Center for Satellite Data Assimilation, Camp Springs, Maryland

RUSS E. TREADON

National Centers for Environmental Prediction, and Joint Center for Satellite Data Assimilation, Camp Springs, Maryland

ABSTRACT

Observing system experiments are used to quantify the contributions to the forecast made by conventional in situ and remotely sensed satellite data. The impact of each data type is assessed by comparing the analyses and forecasts based on an observing system using all data types. The analysis and forecast model used for these observing system experiments is the National Centers for Environmental Prediction (NCEP) Global Data Assimilation/Forecast System (GDAS/GFS). The case studies chosen consist of 45-day periods during January–February 2003 and August–September 2003. During these periods, a T254–64 layer version of NCEP's Global Spectral Model was used. The control run utilizes NCEP's operational database and consists of all data types routinely assimilated in the GDAS. The two experimental runs have either all the conventional in situ data denied (NoCon) or all the remotely sensed satellite data denied (NoSat). Differences between the control and experimental runs are accumulated over the 45-day periods and analyzed to demonstrate the forecast impact of these data types through 168 h. Anomaly correlations, forecast impacts, and hurricane track forecasts are evaluated for both experiments. Anomaly correlations of geopotential height are evaluated over the polar caps and midlatitudes of both the Northern and Southern Hemispheres for spectral waves 1–20. Forecast impacts related to conventional meteorological parameters are evaluated. The parameters examined include geopotential height, precipitable water, temperature, the u component of the wind, wind vector differences, and relative humidity. Comparisons are made on multiple pressure levels extending from 10 to 1000 hPa. Hurricane track forecasts are evaluated during August and September for both the Atlantic and eastern Pacific basins. The results demonstrate a positive forecast impact from both the conventional in situ and remotely sensed satellite data during both seasons in both hemispheres. The positive forecast impacts from the conventional and satellite data are of similar magnitude in the Northern Hemisphere; however, the contribution to forecast quality from satellite data is considerably larger than the conventional data in the Southern Hemisphere. The importance of satellite data also generally increases at longer forecast times relative to conventional data. Finally, the accuracy of hurricane track forecasts benefits from the inclusion of both conventional and satellite data.

Corresponding author address: James A. Jung, NOAA Science Center, 5200 Auth Rd., Camp Springs, MD 20746-4304.
E-mail: jim.jung@noaa.gov

1. Introduction

A diagnostic evaluation of all data being used by operational data assimilation systems is vital if the full impacts of the numerous data sources available today are to be realized. If these types of experiments are not conducted, the integrated influence of each data type will never be understood or identified.

A study of this type also helps delineate the relative importance of data from the Geostationary Operational Environmental Satellites (GOES) and Polar-orbiting Operational Environmental Satellites (POES). The results are of interest to personnel at the National Centers for Environmental Prediction (NCEP) developing future assimilation methods. The results are also of interest to Global Forecast System (GFS) users trying to assess the relative importance of different data types in an operational global model.

A unique aspect of this work, afforded by the Joint Center for Satellite Data Assimilation (JCSDA) and NCEP, is the ability to conduct impact studies at the operational resolution of the time. Until recently, limited resources required that studies covering several seasons be completed at reduced spatial and vertical resolutions. This limitation restricted the conclusions that could be reached with respect to the operational configurations.

This study's goal is to investigate the overall forecast impact of conventional in situ data and remotely sensed satellite data used in the NCEP Global Data Assimilation System (GDAS) for extended periods during the two opposite seasons. This work is similar to observing system experiments (OSEs) conducted with the European Centre for Medium-Range Weather Forecasts (ECMWF) global model by Kelly (1997) and is complementary to the Zapotocny et al. (2000, 2002, 2005a,b) work using the NCEP operational regional model.

In contrast to previous work using the NCEP Eta Data Assimilation System (EDAS; Zapotocny et al. 2000, 2002, 2005a,b), this study investigates the impacts in NCEP's global analysis and forecast system. Evaluation of data impacts in this global system are more straightforward than in regional experiments since there are no effects from lateral boundaries, as was the case with the operational EDAS.

The paper is structured as follows. Section 2 briefly describes the GDAS/GFS version used for this study and the methods used to run the experiments. Section 3 discusses the diagnostics used to evaluate the forecast impacts. Section 4 presents the impact results for the two data sources investigated through 7 days of model forecasts. The overall denial results are summarized in section 5.

2. The model and data assimilation system

For these experiments we used the complete NCEP operational database of conventional and satellite data. The observations used in this work include upper-air rawinsonde observations of temperature, horizontal wind, and specific humidity; operational Advanced Television Infrared Observation Satellite (TIROS-N; Reale 1995; NOAA 2000) Operational Vertical Sounder (TOVS) (Smith et al. 1979) radiances from the High Resolution Infrared Radiation Sounder (HIRS), the Microwave Sounding Unit (MSU) (Spencer et al. 1990), the Advanced Microwave Sounding Unit (AMSU-A and AMSU-B) sensors (NOAA 2005), ozone information from the Solar Backscatter Ultraviolet (SBUV) sensors (Miller et al. 1997); Defense Meteorological Satellite Program (DMSP) Special Sensor Microwave Imager (SSM/I) surface wind speed (Alishouse et al. 1990); derived surface winds from the Quick Scatterometer (Quikscat; Yu and McPherson 1984); atmospheric motion vectors from geostationary satellites (Menzel et al. 1998); aircraft observations of wind and temperature; land surface reports of surface pressure; and oceanic reports of surface pressure, temperature, horizontal wind, and specific humidity. Keyser (2001a, 2001b, 2003) provides an excellent overview of data types provided to NCEP on a daily basis and used operationally for the experiments of this study. The conventional satellite data denied in these experiments are summarized in Tables 1 and 2, respectively.

The NCEP assimilation system consists of a first or "early" cycle with a 2.5-h cutoff. The analyses for this cycle are centered on 0000, 0600, 1200, and 1800 UTC and are followed by a 384-h forecast. Consistent with the operational GDAS/GFS of the time, the model resolution starts at T254L64, is then is reduced to T170L42 at 84 h, and finally it is reduced to T126L28 at 180 h. For this study, only the 0000 UTC forecasts were run out to 384 h. The analysis is repeated later (+6 h) to provide the "final" analysis for the 6-h forecast for the next early cycle first guess. This "final" analysis includes data that had missed the previous "early" cutoff.

a. The global spectral model

Comprehensive documentation of the GFS was completed by the National Meteorological Center (NMC) (now NCEP) Development Division in 1988 and can be found online (http://wwwt.emc.ncep.noaa.gov/gmb/wd23ja/doc/web2/tocold1.html). Subsequent model developments after completion of the above documentation have been summarized by Kanamitsu (1989), Kal-

TABLE 1. In situ data denied within the NCEP GDAS for this study. Mass observations (temperature and moisture) are shown in the left-hand column and wind observations are shown in the right-hand column.

Rawinsonde temperature and humidity	Rawinsonde u and v
AIREP and PIREP aircraft temperatures	AIREP and PIREP aircraft u and v
ASDAR aircraft temperatures	ASDAR aircraft u and v
Flight-level reconnaissance and dropsonde temperature, humidity, and station pressure	Flight-level reconnaissance and dropsonde u and v
MDCARS aircraft temperatures	MDCARS aircraft u and v
Surface marine ship, buoy, and C-MAN temperature, humidity, and station pressure	Surface marine ship, buoy, and C-MAN u and v
Surface land synoptic and METAR temperature, humidity, and station pressure	Surface land synoptic and METAR u and v
Ship temperature, humidity, and station pressure	Wind profiler u and v
	NEXRAD vertical azimuth display u and v
	Pibal u and v

AIREP = aircraft report.
ASDAR = Aircraft to Satellite Data Relay system.
C-MAN = Coastal-Marine Automated Network.
MDCARS = Meteorological Data Collection and Reporting System.
METAR = aviation routine weather report.
NEXRAD = Next-Generation Doppler Radar.
Pibal = pilot balloon.
PIREP = pilot report.

nay et al. (1990), and Kanamitsu et al. (1991). More recent updates to the radiation, surface layer, vertical diffusion, gravity wave drag, convective precipitation, shallow convection, and nonconvective precipitation

TABLE 2. Satellite data denied within the NCEP GDAS for this study.

HIRS sounder radiances	SBUV ozone radiances
MSU radiances	QuikSCAT surface winds
AMSU-A radiances	GOES atmospheric motion vectors
AMSU-B radiances	Atmospheric motion vectors from *GMS-5* until May 2003 then *GOES-9*
GOES sounder radiances	Meteosat atmospheric motion vectors
SSM/I precipitation rate	SSM/I surface wind speed
TRMM precipitation rate	

GMS = Geostationary Meteorological Satellite.
TRMM = Tropical Rainfall Measuring Mission.

can also be found online (http://sgi62.wwb.noaa.gov:8080/research/SONGYU/doc/physmrf1.html). The most recent information about the GFS atmospheric model (2003) is available from NCEP (or online at http://www.emc.ncep.noaa.gov/officenotes/newernotes/on442.pdf). A summary of GFS changes and references up to and past the dates of this study are available in an "updates" log of changes online (at both http://www.emc.ncep.noaa.gov/gmb/moorthi/gam.html and http://www.emc.ncep.noaa.gov/gmb/STATS/html/model_changes.html).

For these denial experiments, the 20 November 2003 operational version and resolution of the GFS were used. A horizontal resolution of 254 spectral triangular waves (T254) was used with a Gaussian grid of 768 × 384 or approximately equal to 0.5° × 0.5° latitude and longitude. The vertical domain ranges from the surface to approximately 0.27 hPa and is divided into 64 unequally spaced sigma layers with enhanced resolution near the bottom and top of the model domain. There are 15 layers below 800 hPa and 24 layers above 100 hPa. The time integration is leapfrog for nonlinear advection terms and semi-implicit for gravity waves and the zonal advection of vorticity and moisture. The time step is 7.5 min for the computation of the dynamics and physics, except that the full calculation of longwave radiation is done once every 3 h and for shortwave radiation it is performed every hour. The long- and shortwave radiation tendencies from these "full" computations are applied linearly every time step as explained in Chou (1992).

b. The spectral statistical interpolation

The analysis scheme is a three-dimensional variational data assimilation (3DVAR) scheme cast in spectral space and is referred to as the Spectral Statistical Interpolation (SSI) algorithm (Derber et al. 1991: Parrish and Derber 1992). With this type of analysis system, the incorporation of radiances directly into the analysis and assimilation system has become practical. The analysis becomes a 3D retrieval of mass, momentum, and moisture fields derived from all available data including the radiances. In October 1995 the direct use of clear and cloud-free satellite radiances in the construction of mass, momentum, and moisture fields was first introduced (Caplan et al. 1997). The methodology for using the radiance data (including the bias correction, ozone analysis, skin temperature, and quality control) is described in Derber and Wu (1998) with the latest upgrades described in Derber et al. (2003). The Joint Center for Satellite Data Assimilation (JCSDA) Community Radiative Transfer Model (CRTM) de-

scribed in Kleespies et al. (2004) has been incorporated into the SSI to improve radiance assimilation.

The SSI uses a thinning routine that identifies the optimal radiance profile for each satellite sensor type (AMSU, HIRS, MSU, etc.) in a predesignated grid box. The optimal radiance profile is determined by its departure from the model background temperature, distance from the center of the grid box, temporal departure from the assimilation time, and surface features (ocean, land, ice).

A hurricane relocation system has been part of NCEP's analysis system since 2000 (Liu et al. 2000). The hurricane relocation algorithm moves the hurricane vortex in the model first-guess field to the observed location before the SSI updates the analysis and is explained by Kurihara et al. (1995). If the vortex is too weak in the guess field, a bogus vortex is added to the SSI data analysis as explained by Lord (1991).

3. Experimental design

Diagnostics presented here include statistics commonly used by NCEP and other NWP centers world wide. The computation of all anomaly correlations for forecasts produced by the GFS are completed using code developed and maintained at NCEP. NCEP (NWS 2006) provides a clear description of the method of computation while Lahoz (1999) presents an overall description of what the anomaly correlation is typically used for. The fields being evaluated, which are truncated to only include spectral wavenumbers 1–20, are limited to the zonal bands 60°–90° and 20°–80° for each hemisphere and a tropical belt within 20° of the equator (20°N–20°S).

The NCEP–National Center for Atmospheric Research (NCAR) reanalysis fields (Kistler et al. 2001) are used for the climate component of the anomaly correlations. This reanalysis was run at a resolution of T62L28. The output grids were reduced to $2.5° \times 2.5°$ horizontal resolution and to rawinsonde mandatory levels. To calculate anomaly correlations, the output grids from the control and both experiments were reduced to this $2.5° \times 2.5°$ horizontal resolution using the GFS postprocessor.

Another diagnostic used here is the root-mean square (RMS) of the forecast impact (FI), which is discussed further by Zapotocny et al. (2005a). For this study, a series of two-dimensional FI results are presented as the positive–negative impact provided by the denial of a particular data type. The geographic distribution of FI shown in section 4b for a specific pressure level is evaluated using

$$ \mathrm{FI}(t, z) = 100 \times \left[\frac{\sqrt{\dfrac{\sum\limits_{i=1}^{X} (D_i' - A_i')^2}{X}} - \sqrt{\dfrac{\sum\limits_{i=1}^{X} (C_i' - A_i')^2}{X}}}{\sqrt{\dfrac{\sum\limits_{i=1}^{X} (C_i' - A_i')^2}{X}}} \right]. \tag{1} $$

The variables C and D are the control and denied forecasts, respectively. The variable A is the 0-h GDAS control analysis containing all data types, which is valid at the same time as the forecasts. Here, N is the number of diagnostic days.

The vertical cross-sectional plots shown in section 4c are evaluated using

$$ \mathrm{FI}(x, y) = 100 \times \left[\frac{\sqrt{\dfrac{\sum\limits_{i=1}^{N} (D_i - A_i)^2}{N}} - \sqrt{\dfrac{\sum\limits_{i=1}^{N} (C_i - A_i)^2}{N}}}{\sqrt{\dfrac{\sum\limits_{i=1}^{N} (C_i - A_i)^2}{N}}} \right], \tag{2} $$

where X is the number of horizontal grid points and A', C', and D, are the area-weighted values of A, C, and D defined in (1). The area ratio weights the grid points to account for the reduction in area as the grid boxes approach the poles. The area ratio weighting is defined as

$$ A_i' = A_i \times \frac{\sin\left(\phi_i + \dfrac{\Delta}{2}\right) - \sin\left(\phi_i - \dfrac{\Delta}{2}\right)}{2 \sin\left(\dfrac{\Delta}{2}\right)}, \tag{3} $$

where ϕ is the latitude of grid point i and Δ is north–south resolution of the grid box. The numerator is the relative size of the grid box. The denominator is the relative size of a grid box at the equator. The FI is then averaged over the number of days by using

$$ F_t = \frac{\sum\limits_{i=1}^{N} \mathrm{FI}(t, z)}{N}, \tag{4} $$

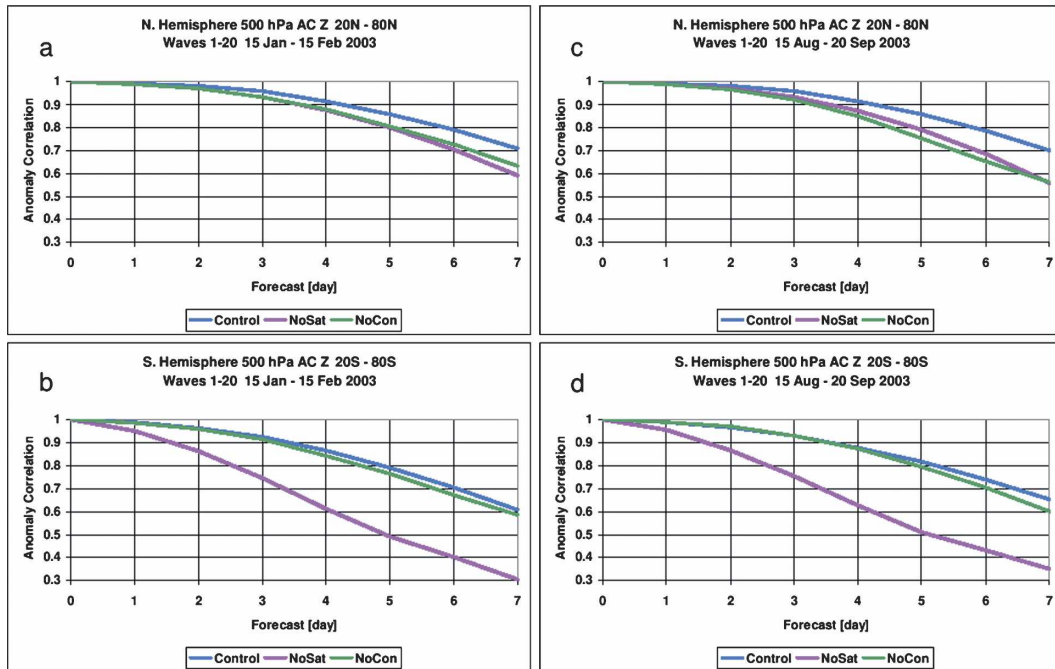where FI is from (2) and N is the number of diagnostic days.

FIG. 1. Anomaly correlation for days 0–7 for 500-hPa geopotential height in the zonal band 20°–80° latitude for each hemisphere and season. The control simulation is shown in blue, while the NoSat and NoCon denial experiments are shown in magenta and green, respectively. For all panels the results have been truncated to only show results less than or equal to wavelength 20: (a) Northern Hemisphere (NH) 15 Jan–15 Feb 2003, (b) Southern Hemisphere (SH) 15 Jan–15 Feb 2003, (c) NH 15 Aug–20 Sep 2003, and (d) SH 15 Aug–20 Sep 2003.

The first terms on the right-hand side enclosed by parentheses in (1) and (2) can be considered to be the errors in the denied experiment. The second terms enclosed by parentheses in (1) and (2) can be considered to be the errors in the control forecast. Dividing by the error of the control forecast normalizes the results. Multiplying by 100 provides a percent improvement–degradation with respect to the RMS error of the control forecast. A positive forecast impact means the control forecast compares more favorably to its corresponding analysis with the data type excluded.

All FI diagnostics were computed from grids generated by NCEP's postprocessing package. These grids have a 1° × 1° horizontal resolution and have 26 vertical isobaric surfaces. None of the fields have been smoothed during calculating or plotting.

All diagnostics exclude the first 15 days of each seasonal time period. This delay in evaluating the statistics allows for the impact of the denied data to be removed from the model initial conditions. Excluding the first 15 days reduces the two seasonal windows to 32 and 37 days for the Northern Hemisphere winter and summer, respectively. The forecast diagnostics for this paper were also terminated at 168 h to concentrate on the shorter-term forecast impacts.

4. Results

The impacts of the satellite and conventional data on the quality of forecasts made by the GFS for two time periods are explored in detail. The first time period covers 15 January–15 February 2003, the second covers 15 August–20 September 2003. The selection of these time periods enables the diagnostics to sample both summer and winter seasons in each hemisphere. The fields diagnosed in this paper consist of geopotential heights, temperature, u component of the wind, wind vector differences, relative humidity, and vertically integrated precipitable water. Underground grid points on isobaric surfaces intersecting the earth's surface are not included in the evaluations. The impact of satellite and conventional data on hurricane track forecasts are also evaluated. To maximize the number of tropical cyclones available for this study in the Atlantic and eastern Pacific basins, the Northern Hemisphere summer time period was shifted and slightly extended toward the fall season.

a. Anomaly correlations

Figure 1 (see Fig. 3 later as well) presents the anomaly correlations for days 0–7 for the NoSat, No-

Con, and control experiments during 15 January–15 February and 15 August–20 September. The blue line is the control simulation, which closely replicates NCEP operations and includes all data routinely used by the GDAS/GFS. The green line is the anomaly correlation diagnosed from the simulations that removed the conventional data shown in Table 1. The magenta line is the anomaly correlation diagnosed from removing the satellite data shown in Table 2. In these types of denial experiments, the larger the separation between the denied and control experiments anomaly correlations, the greater the importance the removed data have on the quality of the simulation.

The midlatitude 500-hPa Northern Hemisphere geopotential height anomaly correlations for the control and two experiments shown in Fig. 1a indicate that the control simulation has the highest anomaly correlation every forecast day after the first day. In fact, at day 5 the control anomaly correlation is just slightly greater than 0.85. The NoCon and NoSat experiments produce lower and very similar anomaly correlations through day 5. After day 5, the NoSat denial anomaly correlation begins to decrease faster than the NoCon anomaly correlation. These results suggest that the NoCon and NoSat data types are of nearly equal importance to forecast quality out to day 5 for midlatitudes of the Northern Hemisphere during January–February 2003.

Figure 1b presents the midlatitude Southern Hemisphere anomaly correlation results for the NoSat and NoCon denials for the January–February time period. Similar to Fig. 1a, the control (green) simulation produces the highest anomaly correlation for all 7 days. This suggests that the conventional and remotely sensed data both provided some value to forecast quality. However, the forecast quality is much worse in the Southern Hemisphere after removing the satellite data (magenta) than it is in the Northern Hemisphere. This is indicated by the dramatic reduction in anomaly correlation for all simulation days shown in Fig. 1b. In fact, while the control experiment has a Southern Hemisphere day 5 anomaly correlation of 0.79, the day 5 anomaly correlation after removing the satellite data is slightly less than 0.50. Another very noticeable characteristic of the Southern Hemisphere midlatitude results is that the removal of conventional data yields a smaller reduction in the anomaly correlation than in the Northern Hemisphere. The greater impact of satellite data in the Southern Hemisphere is typically attributed to there being considerably less conventional data in that hemisphere. Finally, it is generally accepted that an anomaly correlation of 0.6 or greater provides a positive measure of forecast skill. This suggests that remov-

ing the satellite data in the Southern Hemisphere would decrease the useful forecast time from approximately 7 days to approximately 4 days for this time period.

Figures 1c and 1d present the waves 1–20 anomaly correlations for the midlatitude Northern and Southern Hemispheres, respectively, during the August–September 2003 time period. While some differences are seen, the overall conclusion is the same as in the January–February 2003 results shown in Figs. 1a and 1b. It is interesting to note that a 5-day control forecast (with satellite data) has about the same skill as a 4-day forecast without satellite data in the Northern Hemisphere (Fig. 1c) and a 2.5-day forecast without satellite data in the Southern Hemisphere (Fig. 1d).

Results similar to this NoSat experiment are presented in Kistler et al. (2001). Albeit in a slightly different form, their Fig. 5 presents the Northern and Southern Hemisphere impacts from their "SAT" and "NOSAT" experiments for an older T62–28 layer version of the NCEP global system. Their results show a nearly neutral contribution from the satellite data in the Northern Hemisphere and a very large contribution from satellite data in the Southern Hemisphere; however, some satellite instruments used in this experiment were not available during the Kistler et al. (2001) study.

In addition to documenting NoSat results similar to this experiment, the Kistler et al. (2001) results present a 50+ yr record of the NCEP anomaly correlation for the T62–28 layer reanalysis project. Those results depict an increase in the anomaly correlation of between 0.05 and 0.10 at day 5 in the Southern Hemisphere during the 1990s. While this is for an older version of the GFS and at a reduced resolution, it does support the 0.30 increase in the anomaly correlation at day 5 in the Southern Hemisphere achieved by the addition of satellite data in this study (see Figs. 1b and 1d).

Figure 2 displays the 850-hPa (Figs. 2a and 2b) and 200-hPa (Figs. 2c and 2d) RMS vector differences of the wind during the two time periods. Both of these results are limited to the tropical belt (20°N–20°S), truncated to resolve waves 1–20 and illustrate that the error grows rapidly initially then slows with time. For this statistic, the error has grown from zero initially to 4.5–5 m s^{-1} at day 1. However, the error does not reach 9–10 m s^{-1} until approximately day 4.5. This error growth of rapid at first, then slowing as the integration proceeds has been characteristic of the GFS.

Figure 2 indicates that neither satellite nor conventional data provide a dominant influence for these time periods in the Tropics. In lower levels, the impact of removing the conventional data is more detrimental to
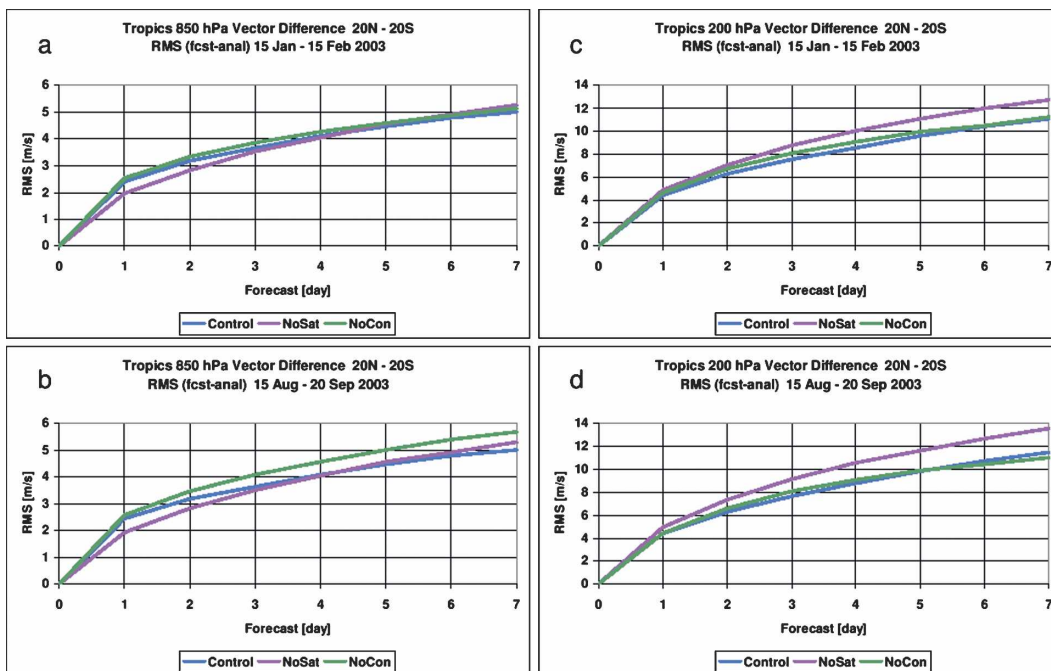
FIG. 2. The (a),(b) 850- and (c),(d) 200-hPa RMS vector differences (m s^{-1}) for days 0–7 in the tropical region (20°N–20°S). The control simulation is shown in blue, while the NoSat and NoCon denial experiments are shown in magenta and green, respectively. For all panels the results have been truncated to only show results less than or equal to wavelength 20.

the forecast quality of the 850-hPa RMS vector difference (Figs. 2a and 2b). At upper levels, the impact from removing satellite data is more detrimental to the RMS vector difference at 200 hPa (Figs. 2c and 2d).

Figure 3 presents the day 0–7 geopotential height anomaly correlations at 500 hPa within the two polar caps (60°–90°) for both seasons. During the Northern Hemisphere winter (Fig. 3a), a nearly equal decrease in anomaly correlation is noticed from the removal of both the conventional and satellite data through day 7, with the day 7 anomaly correlations approximately 0.12 lower for both denials than the control. Less impact is noticed near the poles from the removal of these cumulative data types in the Northern Hemisphere summer (Fig. 3c), with the NoCon and NoSat anomaly correlations close to one another and the control from day 0 to day 7. The removal of satellite data, however, appears to degrade the forecast a little more than does the removal of conventional data.

Relative to its Northern Hemisphere counterpart, a vastly different anomaly correlation distribution is noticed in the Southern Hemisphere polar cap region during each season. In the polar cap region of the Southern Hemisphere, a rapid decrease in anomaly correlation is noticed from the removal of satellite data during both seasons (Figs. 3b and 3d). This is consistent with the

20°–80° anomaly correlations presented in Fig. 1, which partially cover the same geographic area.

Daily 20°–80° zonal band anomaly correlations by season for each denial experiment plus the control simulation are presented in the time series shown in Figs. 4a–d. As expected from the previous results, the control experiment generally has the highest anomaly correlation; however, its daily values fluctuate substantially. The 5-day anomaly correlation standard deviations of the control run for January–February (August–September) are 0.053 (0.068), while the NoCon and NoSat values are 0.055 (0.078) and 0.096 (0.095), respectively. These values represent the average values of both 20°–80° zonal bands and illustrate that there is much more daily variability in anomaly correlation from the removal of these data, particularly the satellite data.

Figure 1a illustrates that the day 5 monthly averaged control anomaly correlation is 0.06 better than the two denials. However, examining the Northern Hemisphere January–February 2003 daily results of Fig. 4a indicates that there are several days when the control anomaly correlation is at or below the NoCon and NoSat level of accuracy. The same is true and even more pronounced for the August–September 2003 Northern Hemisphere results (Fig. 4c). Figures 4b and 4d show that the South-
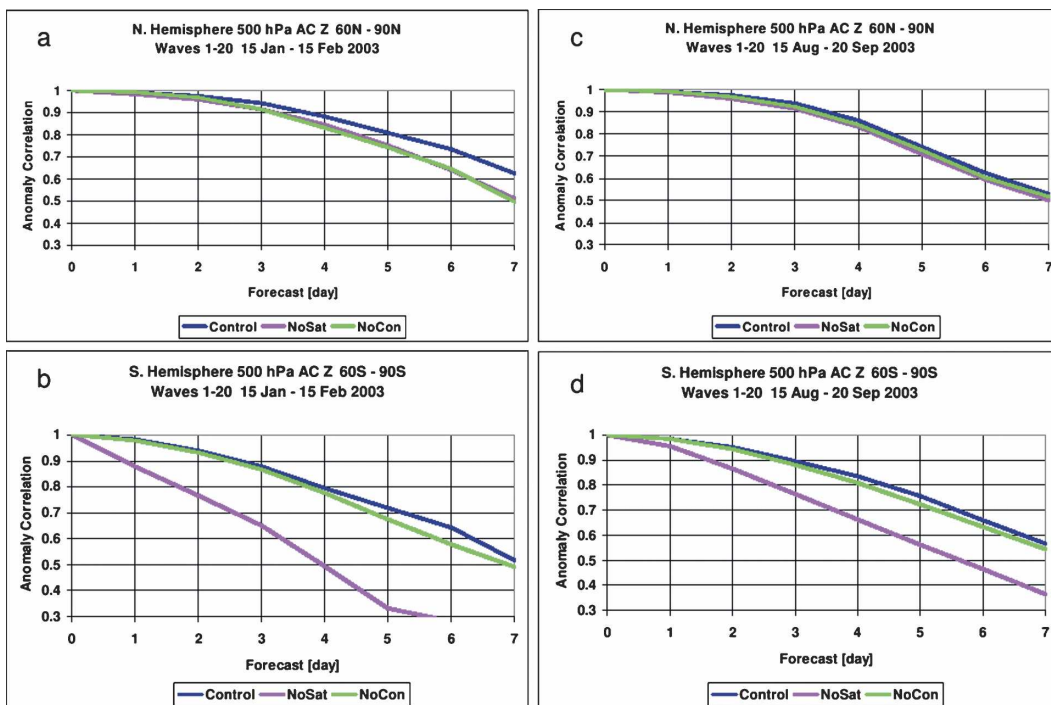
FIG. 3. Anomaly correlation for days 0–7 for 500-hPa geopotential height in the polar cap region (60°–90° latitude) of each hemisphere and season. The control simulation is shown in blue, while the NoSat and NoCon denial experiments are shown in magenta and green, respectively. For all panels the results have been truncated to only show results less than or equal to wavelength 20: (a) NH 15 Jan–15 Feb 2003, (b) SH 15 Jan–15 Feb 2003, (c) NH 15 Aug–20 Sep 2003, and (d) SH 15 Aug–20 Sep 2003.
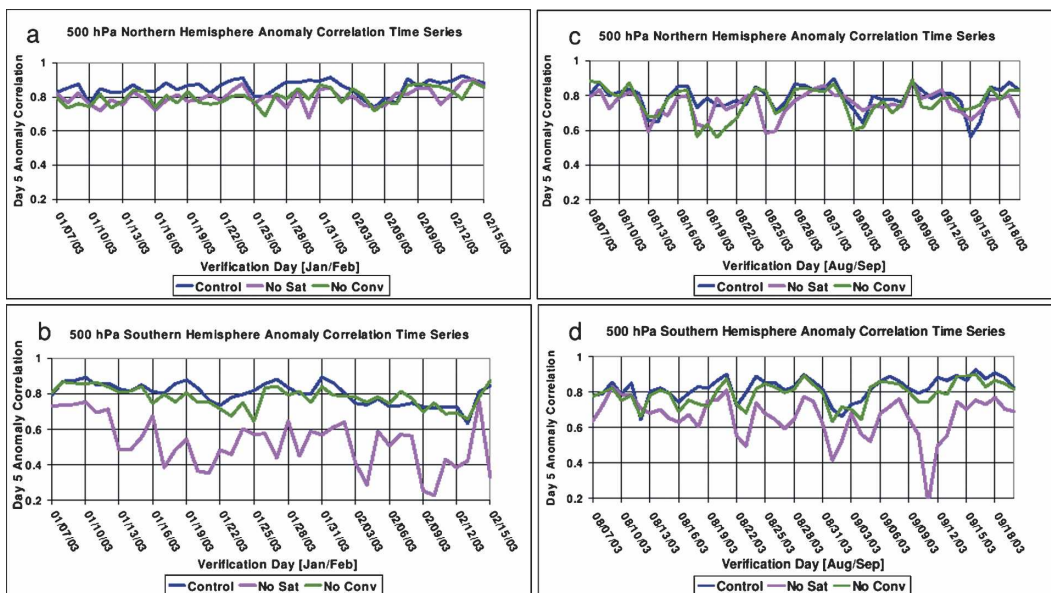

FIG. 4. Time series of the anomaly correlation in the region 20°–80° latitude at day 5 for 500-hPa geopotential height for each hemisphere and season. The control simulation is shown in blue, while the NoSat and NoCon denial experiments are shown in magenta and green, respectively. For all panels the results have been truncated to only show results less than or equal to wavelength 20: (a) NH Jan–Feb 2003, (b) SH Jan–Feb 2003, (c) NH Aug–Sep 2003, and (d) SH Aug–Sep 2003.
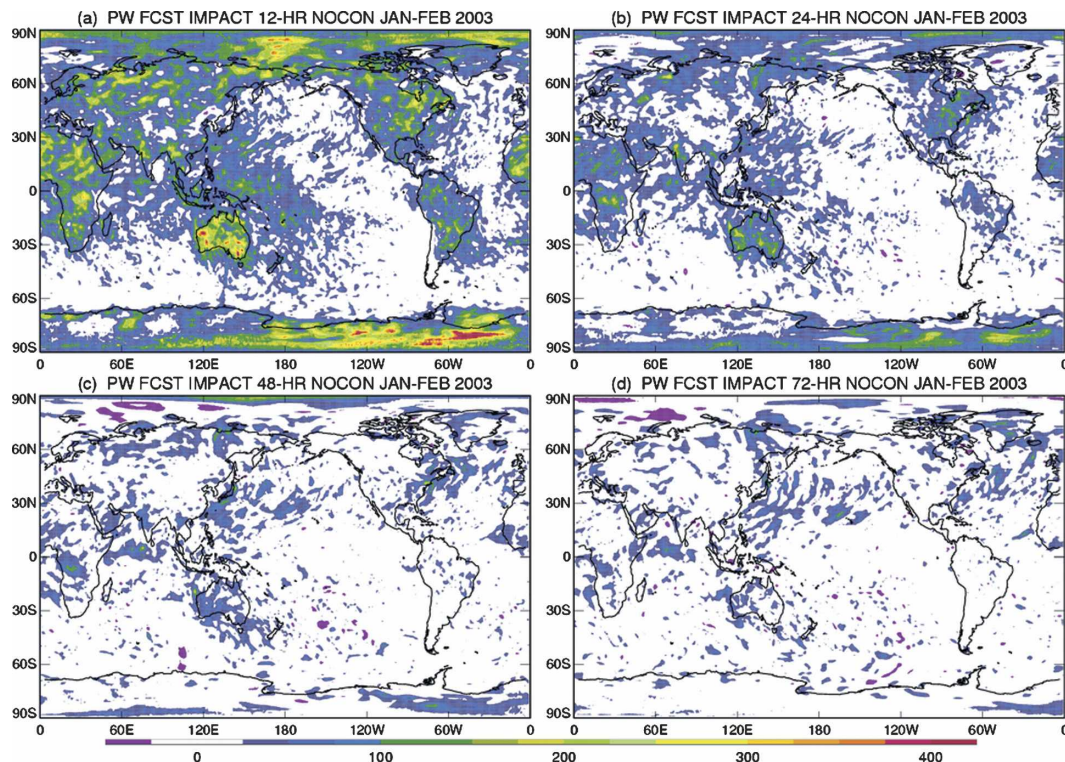
FIG. 5. Geographical distributions of forecast impact from the January–February 2003 time period for vertically integrated precipitable water for the NoCon experiment at forecast hours (a) 12, (b) 24, (c) 48, and (d) 72. The color contour interval is 25% and limited to −50% to +450%. Values outside this range retain the max–min color values. Values closer to zero than ±25% are white.

ern Hemisphere NoSat experiment almost always shows less skill than does the other integrations, especially on 11 September 2003 when its anomaly correlation dips to 0.20.

b. Geographic distributions of forecast impact

Figures 5 and 6 present geographical distributions of forecast impact, determined using (1), for vertically integrated precipitable water. Fields like precipitable water forecasts are very important to the formation and amount of cloud cover, the location and amount of precipitation, and the overall forecast quality. Results from the January–February 2003 NoCon and NoSat experiments for forecast hours 12, 24, 48, and 72 are shown in Figs. 5 and 6. The NoCon 12-h results (Fig. 5a) show the largest forecast impacts in the polar latitudes of each hemisphere as well as over middle- and low-latitude landmasses. Smaller impacts are realized over the eastern Pacific and eastern Atlantic Oceans after 12 h with very limited impact over the Southern Ocean. This is expected due to the sparse coverage of conventional data over the oceans. The largest landmass impacts are over Australia and Antarctica, where the geographic

outlines of the continents are apparent. Subsequently, there is a marked decrease in forecast impact of precipitable water by 24 h (Fig. 5b). The largest impacts are still realized over much of the landmasses, for example, Antarctica, eastern North America, Australia, and Africa at this time. Further decreases in forecast impact are diagnosed by 48 and 72 h, with the generation of small regions of negative impact near the North Pole by 72 h.

Figure 6 presents the January–February 2003 NoSat precipitable water forecast impacts at forecast hours 12, 24, 48, and 72. Consistent with the results above, large positive forecast impacts are seen over Antarctica at 12 h. Large positive forecast impacts are also seen over the southern oceans. The smallest impacts are diagnosed over the interior of Asia and North America, where little if any forecast impact is realized at 12 h. Comparing Figs. 5 and 6 reveals that the NoSat experiment shows satellite data has a markedly more positive impact throughout the 72-h period than does conventional data.

The NoCon and NoSat forecast impacts for precipitable water during August–September 2003 are shown
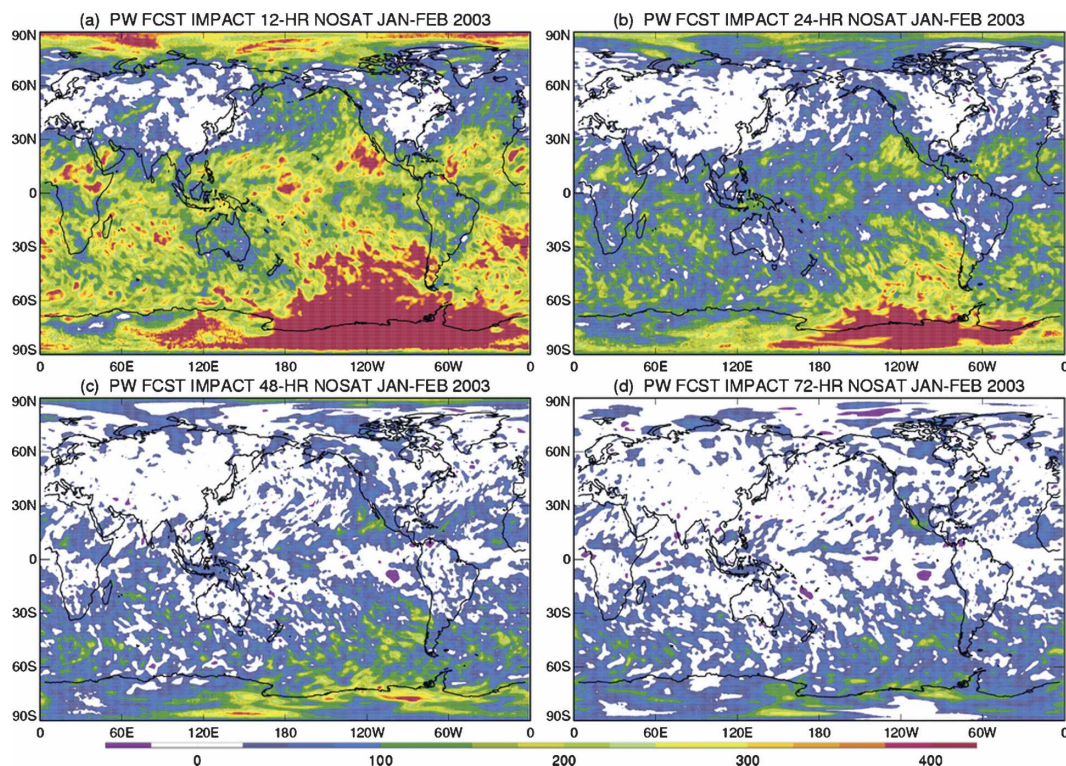
FIG. 6. As in Fig. 5 but for the NoSat experiment.

in Figs. 7 and 8, respectively. During the Northern Hemisphere summer the NoCon 12-h precipitable water forecast impacts (Fig. 7a) are largest over northern Africa, Asia, and North America. To some extent, this represents a shift of hemispheres from the NoCon 12-h results shown in Fig. 5a. Comparing Figs. 6a and 8a, the NoSat forecast impacts are largest near 70°S, 120°W during both time periods. However, the NoSat August–September 2003 results do show some increase in forecast impact over their January–February 2003 counterparts in the northern Pacific Ocean and northern landmasses. Similar to the January–February 2003 results, both the NoCon and NoSat precipitable water forecast impact results decrease sharply from 12 to 24 h, although the NoSat results still indicate small positive impact for all forecasts over the southern oceans.

A forecast field often used to indicate forecast skill is the 500-hPa geopotential heights. Figures 9–12 present the geographic distributions of forecast impacts for this field for the two time periods and experiments examined. Figures 9 and 10 show the January–February 2003 NoCon and NoSat 500-hPa geopotential height results, respectively. For these fields, the same shading is used as for the precipitable water results in Figs. 5–8. Figure 9a shows that the largest positive impact in January–February 2003 for conventional data is over Antarctica.

Secondary maxima appear over northeastern North America and the Arctic Ocean. A large area of relatively small negative forecast impact is found in tropical latitudes west of South America. Elsewhere, the 500-hPa geopotential height forecast impacts from all conventional data during January–February 2003 are, for the most part, neutral. Figures 9b–d indicate that the 12-h forecast impacts decrease rapidly with time, which is consistent with the other verifications presented here.

A very different result is obtained when inspecting the 500-hPa geopotential height forecast impact results from the NoSat experiment during January–February 2003 in Fig. 10. As with the precipitable water results (Fig. 6), the largest impacts of the satellite data are between 50° and 80°S near 120°W. Another less expansive maximum is diagnosed over the Arctic Ocean. Forecasts over the southern oceans and much of the northern Indian Ocean have also improved. While there is a decrease in impact with time from 12 to 72 h, the impact does not fall to the level of those for the NoCon results in Fig. 9.

Figures 11 and 12 are the August–September 2003 geopotential height results for the NoCon and NoSat experiments, respectively. While there are some shifts in the location of both maxima and minima, overall the same conclusions hold for August–September 2003 as
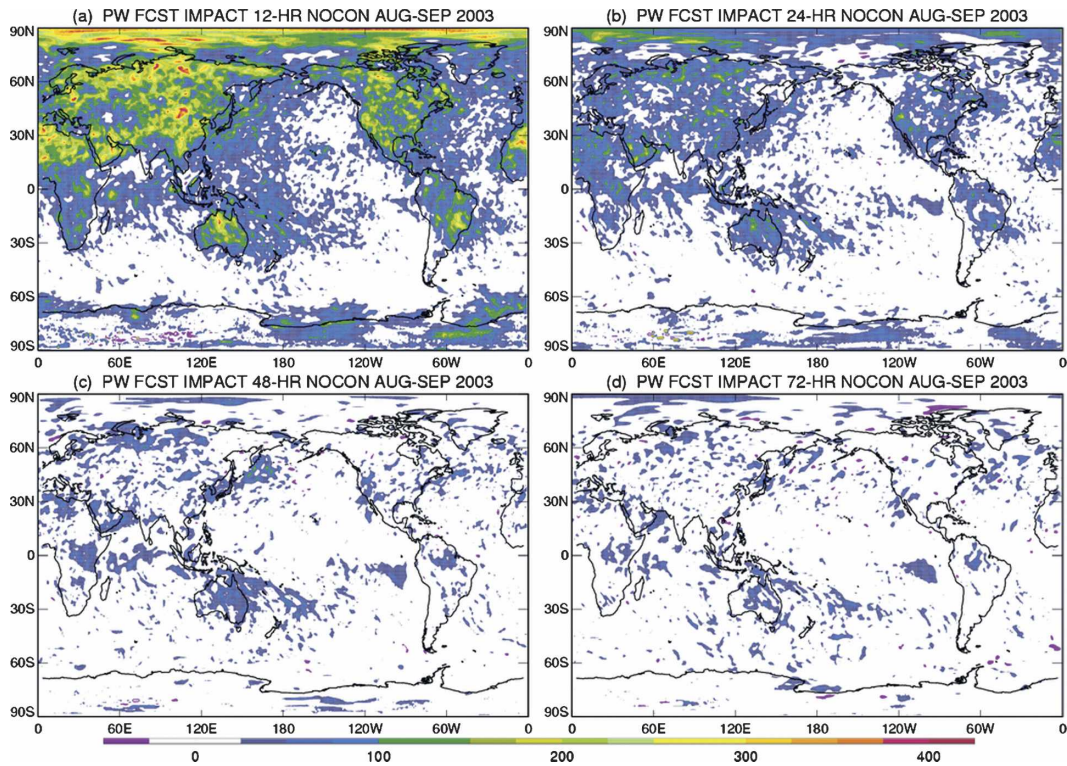
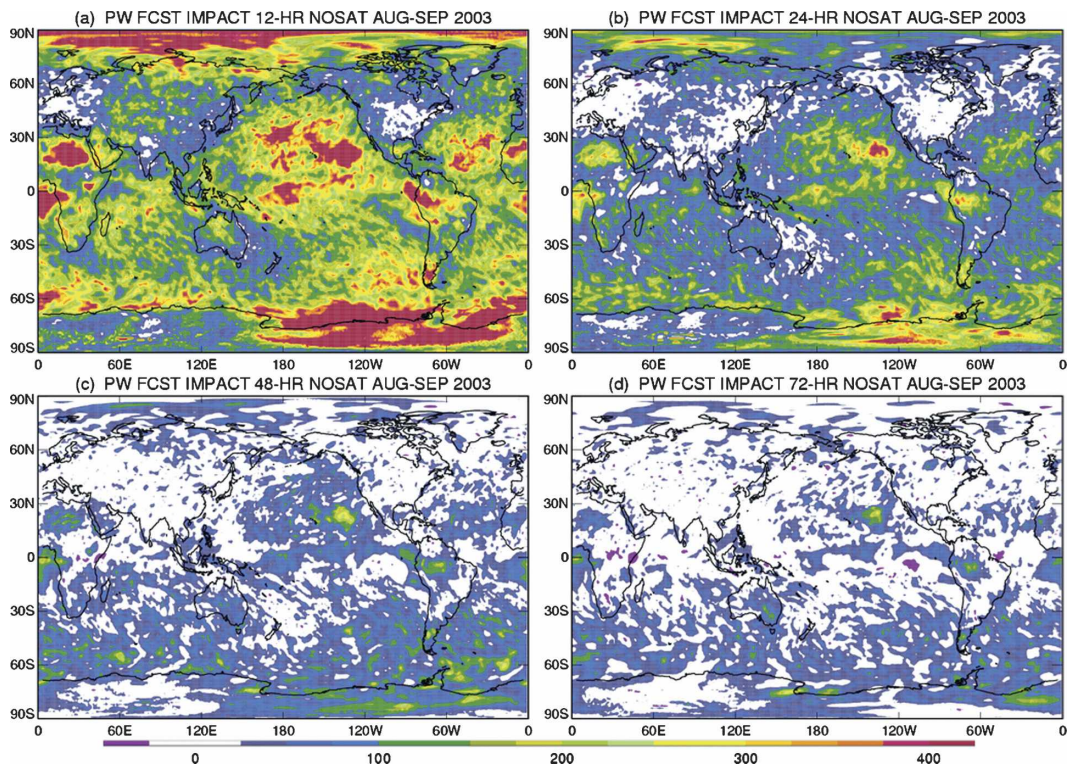FIG. 7. As in Fig. 5 but for the August–September 2003 time period.

FIG. 8. As in Fig. 5 but for the August–September 2003 time period and the NoSat experiment.
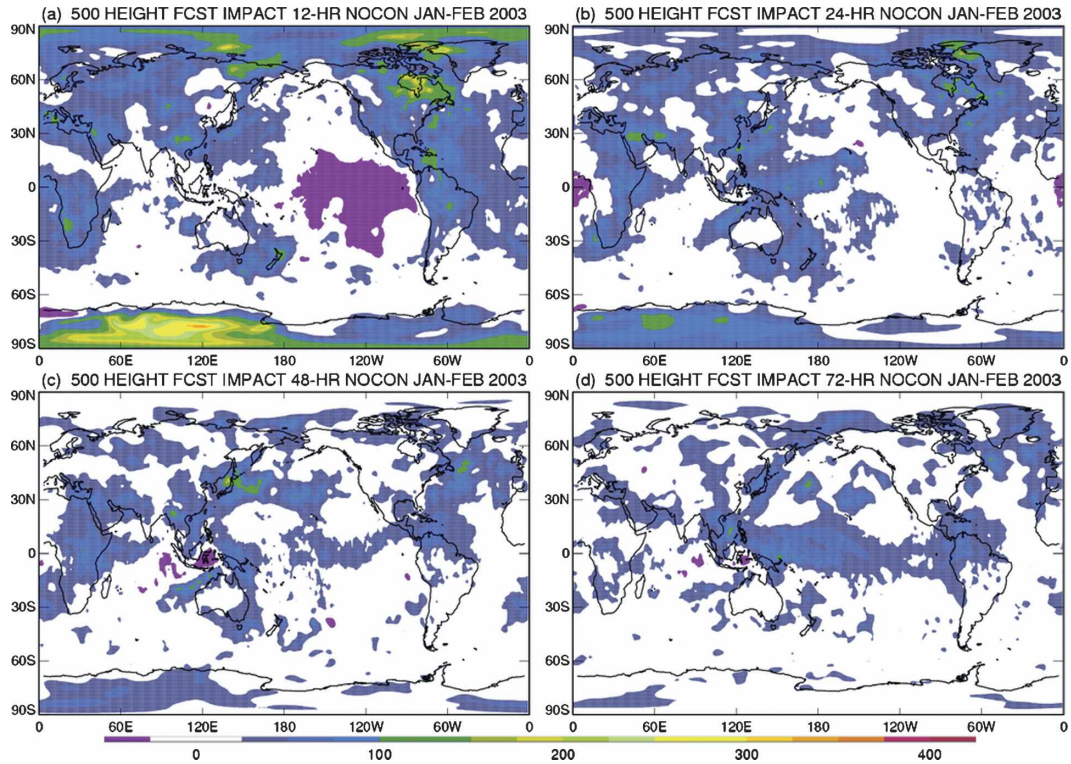
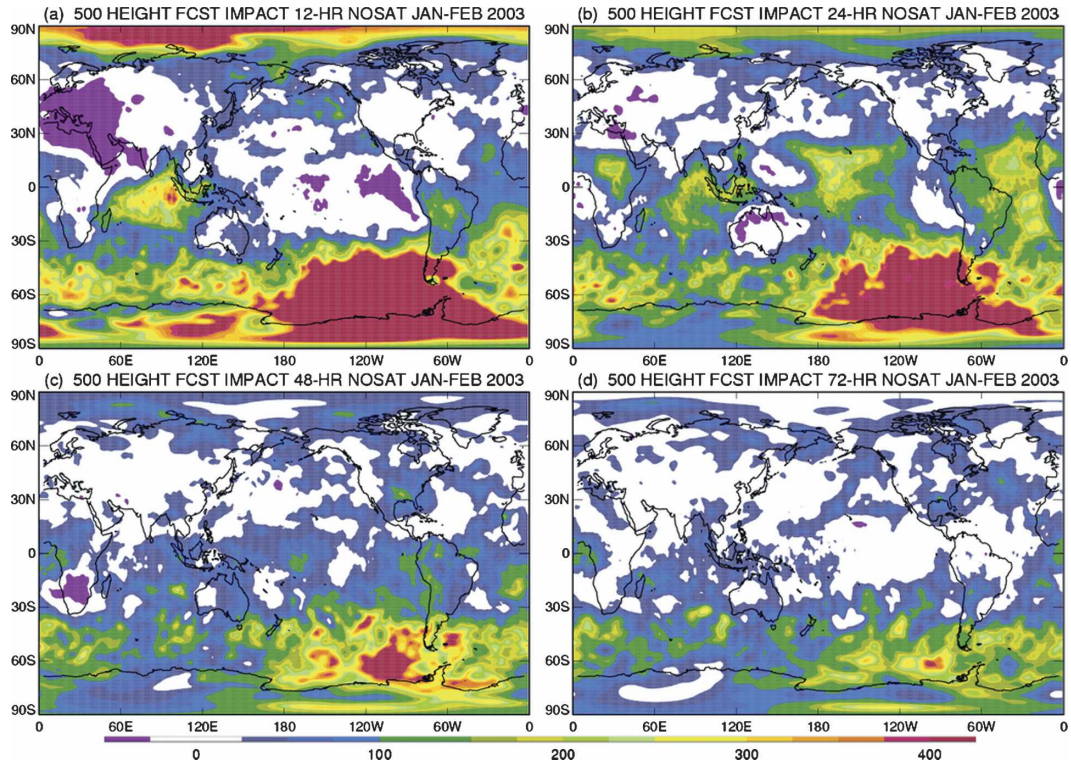FIG. 9. As in Fig. 5 but for the 500-hPa geopotential height.

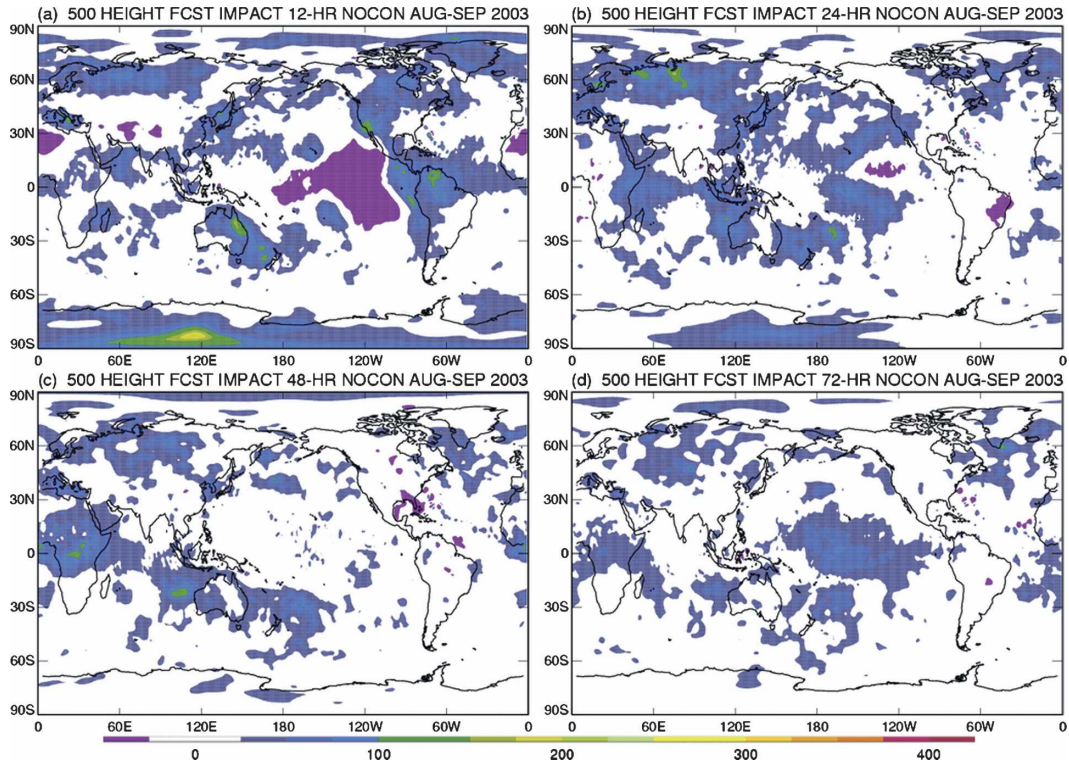FIG. 10. As in Fig. 5 but for the 500-hPa geopotential height and the NoSat experiment.

FIG. 11. As in Fig. 5 but for the 500-hPa geopotential height and the August–September 2003 time period.
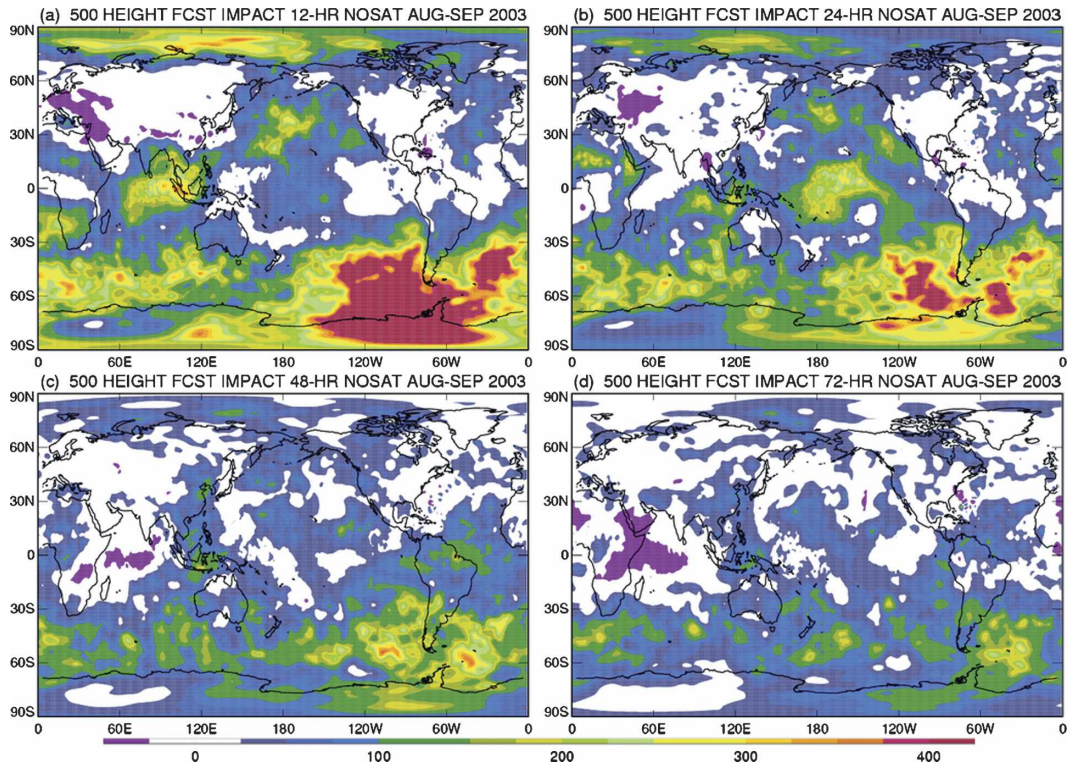

FIG. 12. As in Fig. 5 but for the 500-hPa geopotential height, the August–September 2003 time period, and the NoSat experiment.

were discussed for Figs. 9 and 10 for January–February 2003.

c. Vertical cross sections of forecast impact

Figures 13–18 present vertical cross sections of the temporally and zonally averaged forecast impacts from both the NoSat and the NoCon experiments. The figures were computed using (2) and are partitioned into a global impact (top two panels in each of the figures) as well as hemispheric impacts within the zonal bands 20°–80° in each hemisphere. Forecast impacts from the temperature, u component, and relative humidity are shown for each seasonal time window. Figure 13 shows the January–February 2003 temperature forecast impacts from the NoCon and NoSat denials. Inspection of the plots reveals that the largest impacts are in the stratosphere for each hemisphere, with the Southern Hemisphere displaying the largest impacts. The Southern Hemisphere having the largest impact is consistent with the anomaly correlation scores in Fig. 1.

In the troposphere, all six panels display a systematic decrease of FI with time. In the Northern Hemisphere, the FI has been reduced substantially by 48 h. There is a larger and more persistent Northern Hemisphere FI from the NoCon experiment (Fig. 13b) than from the corresponding Northern Hemisphere NoSat experiment (Fig. 13e). This is in agreement with the zonal band anomaly correlation results in Fig. 1. Contrary to the Northern Hemisphere results shown in Figs. 13b and 13e, the NoSat FI dominates in the global (Figs. 13a and 13d) and Southern Hemisphere (Figs. 13c and 13f) results. This is also consistent with the anomaly correlation results in Fig. 1.

In relation to Figs. 13 and 14, it should be noted that the largest adjustments to model fields from new data often reside in the lower stratosphere. This is true for both hemispheres since the lower stratosphere is where strong temperature inversions exist, thereby creating a region difficult to simulate and verify.

Figures 14 and 15 present the u-component and relative humidity forecast impacts for January–February 2003, respectively. The same general conclusions can be drawn from examining the forecast impact to these state fields as was drawn for temperature in Fig. 13. Specifically, forecast impacts from the NoSat experiment are greater and last longer than the forecast impacts from the NoCon experiment. Moisture FI results are limited to 100 hPa due to inaccuracies in computing saturation at the very cold temperatures found in the lower stratosphere.

Figures 16–18 are the same fields as in Figs. 13–15 except that these are the August–September 2003 results. Similar forecast impact patterns are noticed in

August–September 2003 as during January–February 2003. There are again marked decreases in forecast impact with time and the largest impacts are nearly always found in the lower stratosphere. In general, the temperature and u-component forecast impacts are not as large in August–September as they are in January–February. The moisture forecast impacts are of comparable size during each time period. It may also be noted that low-level and near-surface temperature, u-component, and moisture forecast impacts are degraded more by the removal of satellite data than conventional data in the Southern Hemisphere (see panels c and f in Figs. 16–18). A final point about the zonally and temporally averaged forecast impact results is that the 6-h temporal resolution of the GFS archive used for these experiments is inadequate to resolve the rapid decrease in forecast impact that occurs in the first 12 h of these simulations.

d. Impact of removing satellite and in situ data on hurricane track forecasts

This section examines the impact that removing all satellite and all in situ data has on hurricane track forecasts out to 96 h in both the Atlantic and eastern Pacific basins during the relatively short time period of 15 August–20 September 2004. It is important to note that the hurricane dropsondes were removed as part of the in situ denial experiment. Furthermore, in order for a storm to be used in the diagnostics, the storm must exist in both experiments and the control. If a storm (tropical depression, tropical storm, or hurricane) is not found in the experiments and the control, it is discarded from the statistics. The diagnostics are computed over only one hurricane season, contributing to the small sample size, which must be taken into account when interpreting the results. For completeness, the sample size is shown on the bottom of each panel in Fig. 19. It is also important to note that the sample size is considerably larger in the Atlantic basin for this time period than the Pacific basin, where at 72 and 96 h the sample size is only two storms.

Figure 19 displays the average track error in the GFS forecasts for the control, NoSat, and NoCon experiments. Inspection of Figs. 19a and 19b, which show the average track errors in the Atlantic and Pacific basins, respectively, indicates that both the satellite and in situ data provide improvements to the track forecasts. This is implied from the fact that the control simulation has a lower average track error than either the NoSat or the NoCon experiments.

The gain from using the satellite data is in general larger than the gain from using the in situ data. This is true for all time periods presented, except the 12-h At-
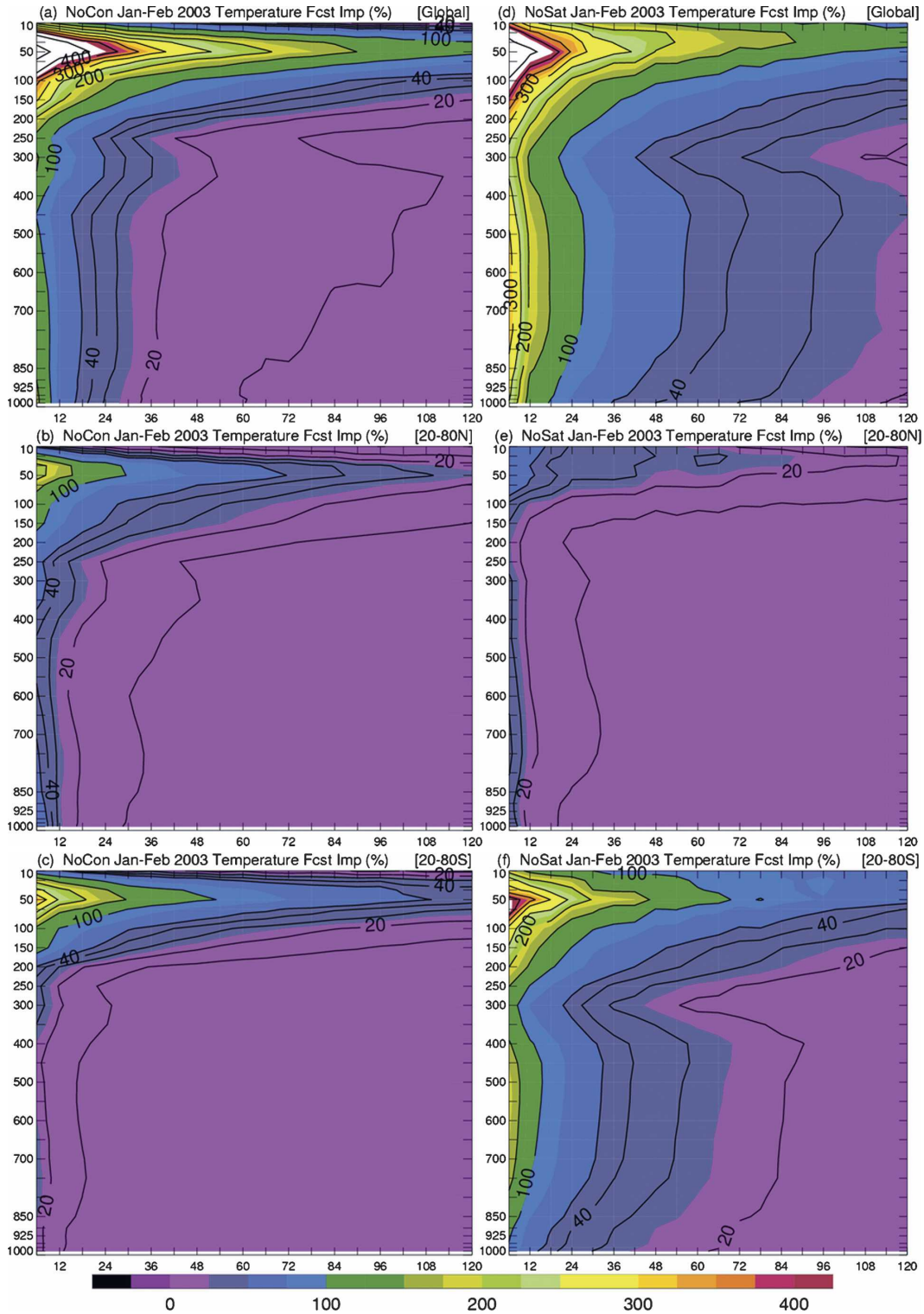
FIG. 13. Cross sections of January–February 2003 forecast impact (%) to temperature as a function of pressure (hPa) and forecast time (h) for (a),(d) the entire globe, (b),(e) 20°–80°N, and (c),(f) 20°–80°S. The NoCon experiment is shown on the left while the NoSat experiment is shown on the right. The colors have a uniform contour interval of 25%. To highlight impacts at smaller percentages, the black contours have a 10% interval from −20% to 50%, a 50% interval from 50% to 500%, and a 150% interval above 500%.
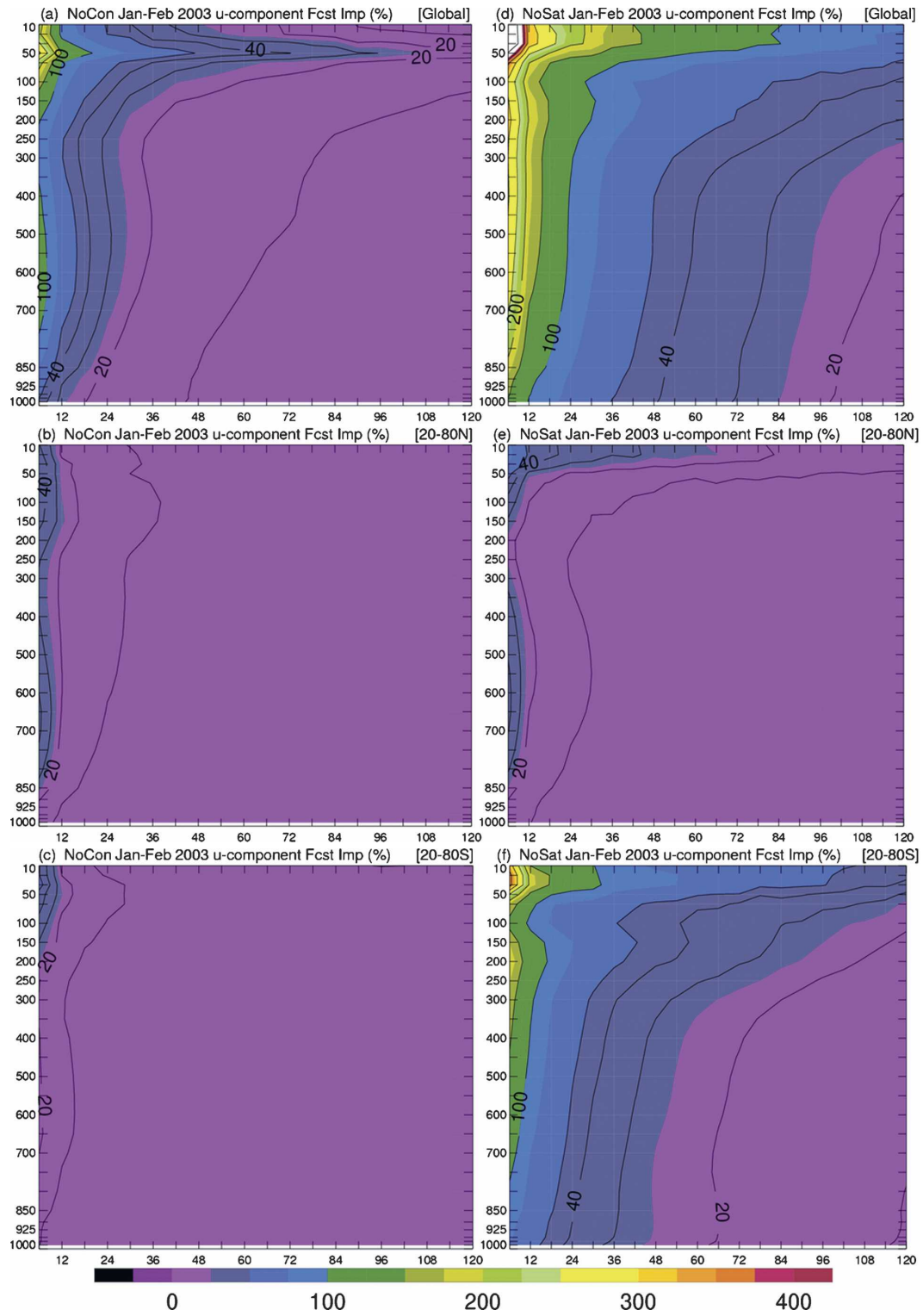
FIG. 14. As in Fig. 13 but for the *u* component of the wind.
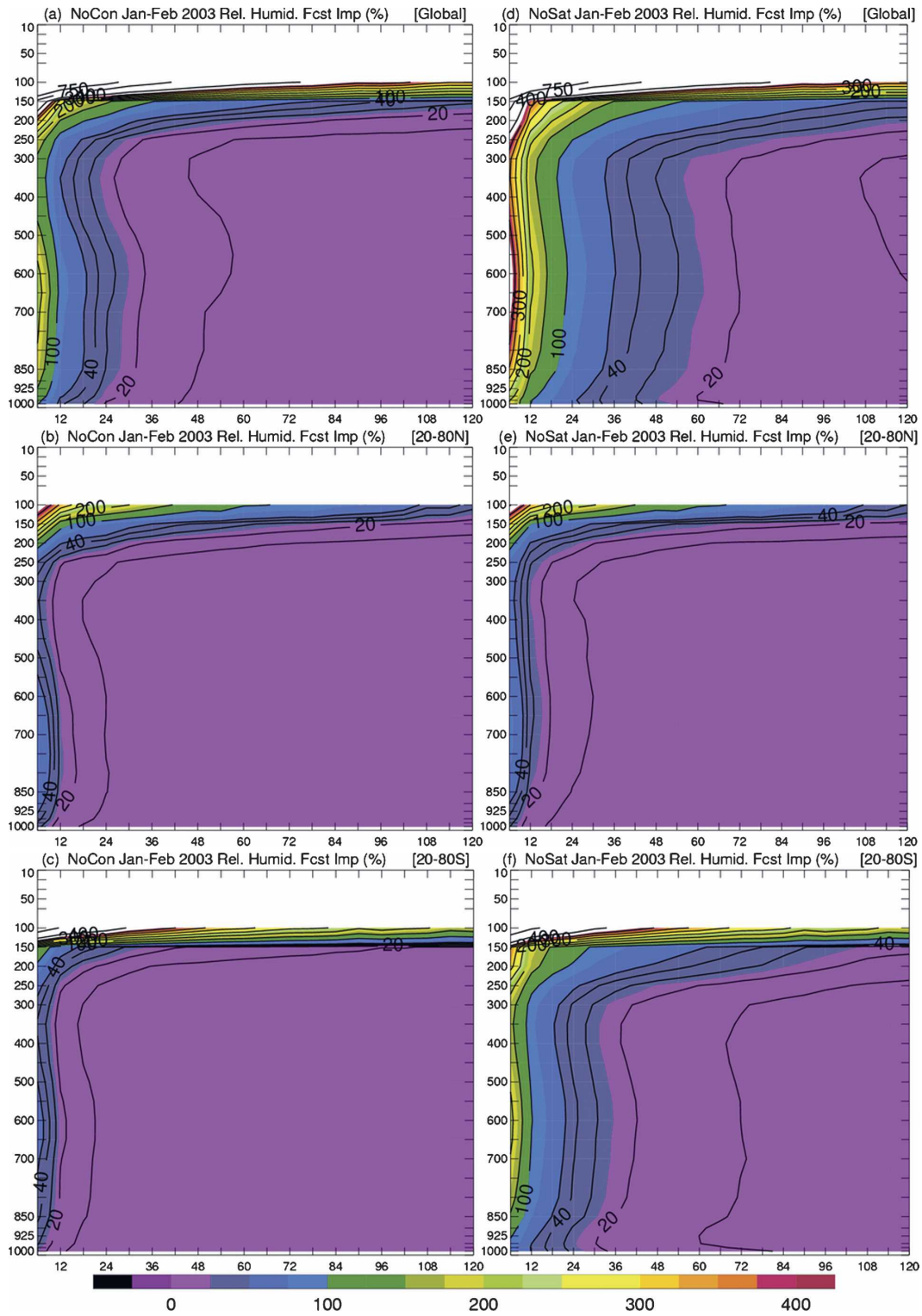
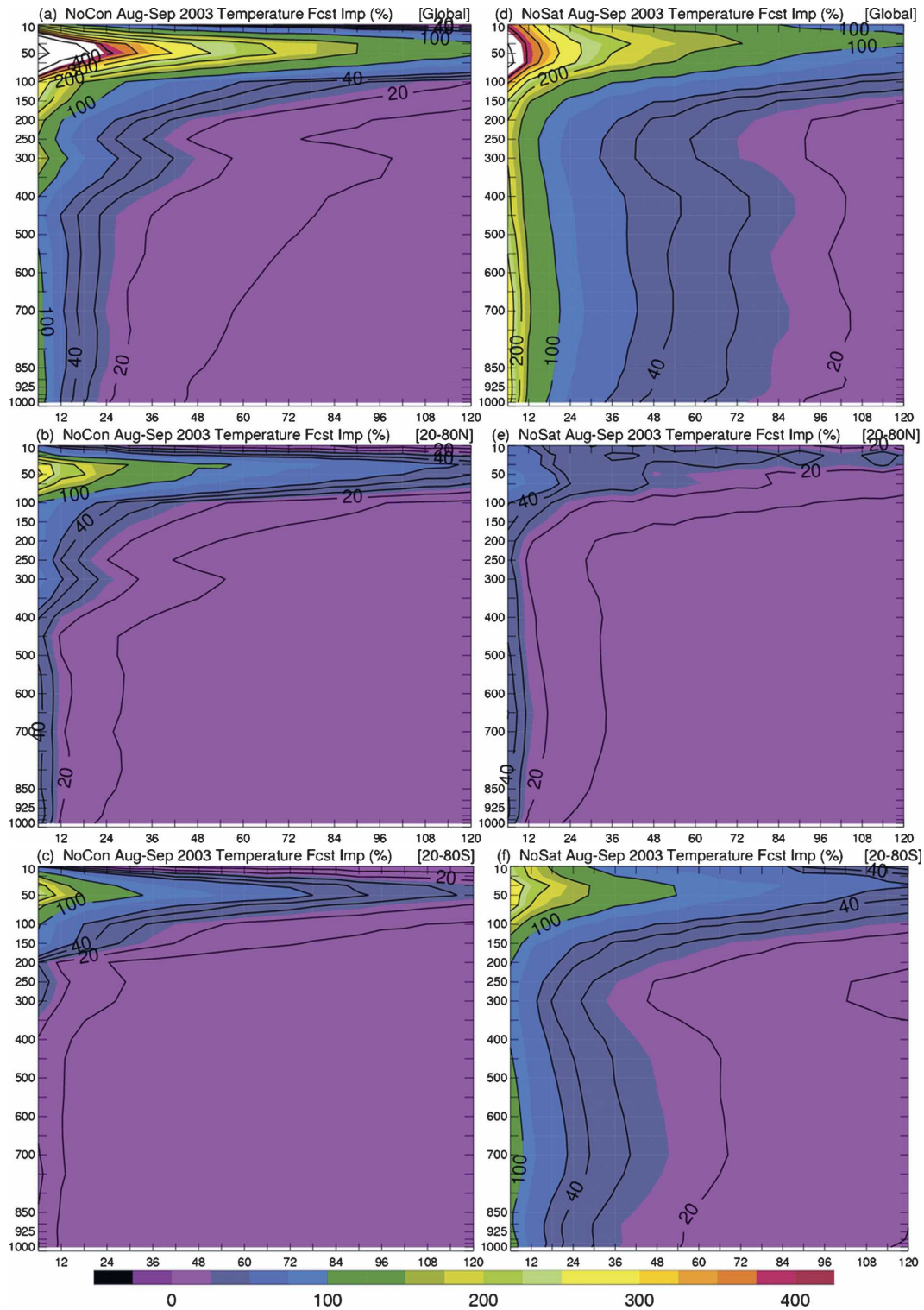FIG. 15. As in Fig. 13 but for relative humidity.

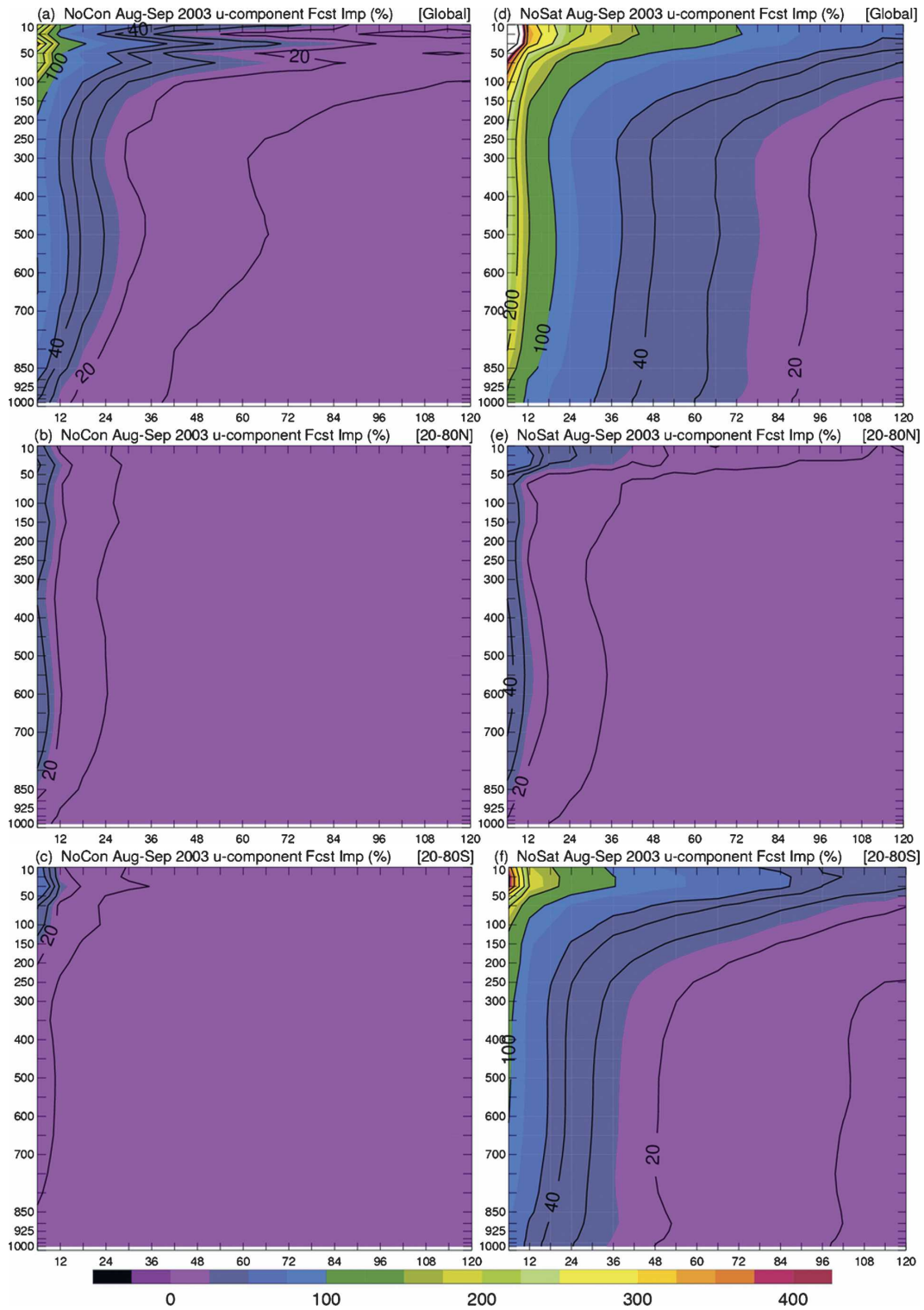FIG. 16. As in Fig. 13 but for August–September 2003.

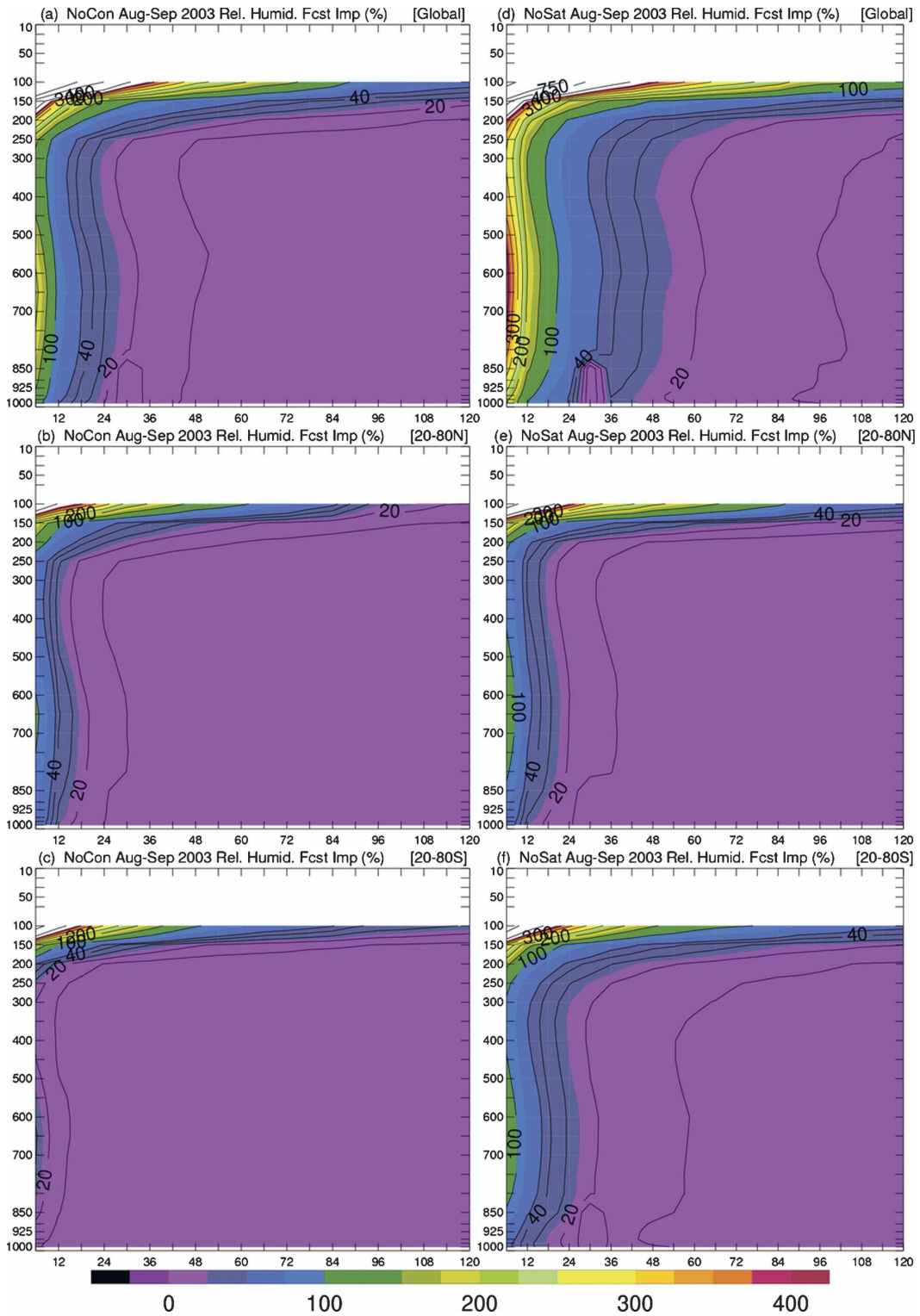FIG. 17. As in Fig. 13 but for August–September 2003 and the *u* component of the wind.

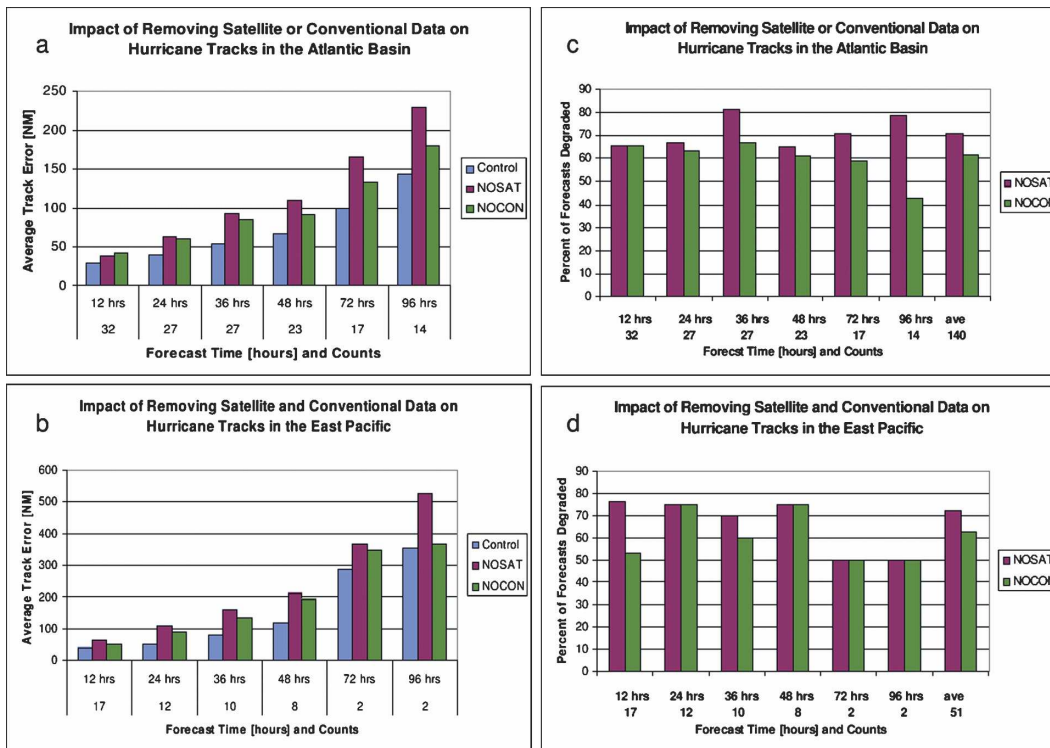FIG. 18. As in Fig. 13 but for August–September 2003 and relative humidity.

FIG. 19. The impact of removing satellite and in situ data on hurricane track forecasts in the GFS during the period 15 Aug–20 Sep 2003. (a),(b) The average track error (n mi) out to 96 h for the control experiment and the NoSat and NoCon denials for the Atlantic and Pacific basins, respectively. (c),(d) The percentage of forecasts that were degraded or improved relative to verification for the NoSat and NoCon denials in the Atlantic and Pacific basins, respectively. A column displaying the 12–96-h average is also shown in (c) and (d).

lantic basin average, where more accurate forecasts are produced from the application of conventional data than from the application of satellite data. The satellite data improve track forecasts in the longer term by more accurately resolving the steering currents in the oceanic regions when the systems are far from the conventional data network.

Figures 19c and 19d show the percent of forecasts during this 2003 time window that were degraded or improved by denying the aggregate satellite and in situ data types. In these two panels values greater than 50% indicate an improvement in track error when the data are used. For completeness, an average of the 12–96-h results is presented on the far right of each panel. In the Atlantic basin the effect of satellite data is to always provide a better forecast than without it. This is also true for the in situ data, except for the 96-h NoCon case where a value of 43% is observed. The remainder of the cases, including the average, demonstrates that approximately 60%–80% of the tracks were more accurate with the inclusion of either data type. It is clear from this study that the addition of both conventional and satellite data improves the track forecasts of tropi-

cal systems in the GFS. Note, however, that the sample size is very small, especially for the 72- and 96-h forecasts.

5. Summary

An observing system experiment (OSE) examining the 0–168-h forecast impact results during 45-day periods in January–February and August–September 2003 has been completed. It quantifies the change in forecast quality in the NCEP GDAS/GFS when all conventional in situ data (NoCon) or all remotely sensed satellite data (NoSat) were removed from the analysis system.

Results indicate that removing the satellite data or conventional data provides comparable forecast degradation through day 7 in the Northern Hemisphere. However, the remotely sensed data are of paramount importance to forecast quality in the Southern Hemisphere. Particularly noteworthy is the very large day 7 anomaly correlation decrease of nearly 0.3 in the Southern Hemisphere after the removal of the satellite data. A further result was that, for fields such as precipitable water and 500-hPa geopotential heights, the

extensive coverage of the positive forecast impact from remotely sensed data was retained much longer than was the positive forecast impact coverage from conventional data. Finally, it was found in this study that both the Atlantic and Pacific basin hurricane track forecasts were degraded when either the conventional data or satellite data were denied from the analysis. In general, the degradation was larger with the removal of satellite data.

As a follow-on to this study, the impacts from the different data types going into the aggregate NoSat and NoCon denials of this study are being examined. This work is using the same time periods and GDAS/GFS version as this study and will be presented as a follow-on to the results discussed here. The work also includes diagnosing the impact of new data types such as atmospheric motion vectors (AMVs) in polar regions from the Moderate Resolution Imaging Spectroradiometer (MODIS), Atmospheric Infrared Radiometer (AIRS) radiances, and ocean surface wind vector measurements from space using WindSAT.

REFERENCES

Alishouse, J. C., S. Snyder, J. Vongsathorn, and R. R. Ferraro, 1990: Determination of oceanic total precipitable water from the SSM/I. *IEEE Trans. Geosci. Remote Sens., 28,* 811–816.

Caplan, P., J. C. Derber, W. Gemmill, S. Hong, H. Pan, and D. F. Parrish, 1997: Changes to the 1995 NCEP operational Medium-Range Forecast model analysis–forecast system. *Wea. Forecasting, 12,* 581–594.

Chou, M.-D., 1992: A solar radiation model for use in climate studies. *J. Atmos. Sci., 49,* 762–772.

Derber, J. C., and W.-S. Wu, 1998: The use of TOVS cloud-cleared radiances in the NCEP SSI analysis system. *Mon. Wea. Rev., 126,* 2287–2299.

——, D. F. Parrish, and S. J. Lord, 1991: The new global operational analysis system at the National Meteorological Center. *Wea. Forecasting, 6,* 538–547.

——, P. Van Delst, X. Su, X. Li, K. Okamoto, and R. Treadon, 2003: Enhanced use of radiance data in the NCEP data assimilation system. *Proc. 13th Int. TOVS Study Conf.,* St. Adele, QC, Canada, IAMAS/ITWG, 52–59. [Available online at http://cimss.ssec.wisc.edu/itwg/itsc/itsc13/proceedings/session1/1_8_derber.pdf.]

Kalnay, E., M. Kanamitsu, and W. E. Baker, 1990: Global numeri-

cal weather prediction at the National Meteorological Center. *Bull. Amer. Meteor. Soc., 71,* 1410–1428.

Kanamitsu, M., 1989: Description of the NMC Global Data Assimilation and Forecast System. *Wea. Forecasting, 4,* 335–342.

——, and Coauthors, 1991: Recent changes implemented into the Global Forecast System at NMC. *Wea. Forecasting, 6,* 425–435.

Kelly, G., 1997: Influence of observations on the operational ECMWF system. *Tech. Proc. of the Ninth Int. TOVS Study Conf.,* Igls, Austria, IAMAS/ITWG, 239–244.

Keyser, D., cited 2001a: Code table for PREPBUFR report types used by the Global GFS. [Available online at http://www.emc.ncep.noaa.gov/mmb/data_processing/prepbufr.doc/table_2.htm.]

——, cited 2001b: Summary of the current NCEP analysis system usage of data types that do not pass through PREPBUFR processing. [Available online at http://www.emc.ncep.noaa.gov/mmb/data_processing/prepbufr.doc/table_19.htm.]

——, cited 2003: Observational data processing at NCEP. [Available online at http://www.emc.ncep.noaa.gov/mmb/data_processing/data_processing/.]

Kistler, R., and Coauthors, 2001: The NCEP–NCAR 50-Year Reanalysis: Monthly means CD-ROM and documentation. *Bull. Amer. Meteor. Soc., 82,* 247–267.

Kleespies, T. J., P. Van Delst, L. M. McMillin, and J. C. Derber, 2004: Atmospheric Transmittance of an absorbing gas. OPTRAN status report and introduction to the NESDIS/NCEP Community Radiative Transfer Model. *Appl. Opt., 43,* 3103–3109.

Kurihara, Y., M. A. Bender, R. E. Tuleya, and R. J. Ross, 1995: Improvements in the GFDL hurricane prediction system. *Mon. Wea. Rev., 123,* 2791–2801.

Lahoz, W. A., 1999: Predictive skill of the UKMO Unified Model in the lower stratosphere. *Quart. J. Roy. Meteor. Soc., 125,* 2205–2238.

Liu, Q., T. Marchok, H.-L. Pan, M. Bender, and S. Lord, 2000: Improvements in hurricane initialization and forecasting at NCEP with the global and regional (GFDL) models. EMC Tech. Procedures Bull. 472, 7 pp.

Lord, S. J., 1991: A bogussing system for vortex circulations in the National Meteorological Center Global Forecast Model. Preprints, *19th Conf. on Hurricane and Tropical Meteorology,* Miami, FL, Amer. Meteor. Soc., 329–330.

Menzel, W. P., F. C. Holt, T. J. Schmit, R. M. Aune, A. J. Schreiner, G. S. Wade, and D. G. Gray, 1998: Application of *GOES-8/9* soundings to weather forecasting and nowcasting. *Bull. Amer. Meteor. Soc., 79,* 2059–2077.

Miller, A. J., and Coauthors, 1997: Information content of Umkehr and SBUV(2) satellite data for ozone trends and solar responses in the stratosphere. *J. Geophys. Res., 102,* 19 257–19 263.

NOAA, cited 2000: NOAA KLM users guide, September 2000 revision. [Available online at http://www2.ncdc.noaa.gov/docs/klm/cover.htm.]

——, cited 2005: NOAA Polar Orbiter Data (POD) user's guide, November 1998 revision. [Available online at http://www2.ncdc.noaa.gov/docs/klm/html/c3/sec3-3.htm.]

NWS, cited 2006: NCEP anomaly correlations. [Available online at http://wwwt.emc.ncep.noaa.gov/gmb/STATS/STATS.html.]

Parrish, D. F., and J. C. Derber, 1992: The National Meteorological Center's Spectral Statistical Interpolation Analysis system. *Mon. Wea. Rev., 120,* 1747–1763.

Reale, A. L., 1995: Departures between derived satellite sound-ings and numerical weather forecasts: Present and future. *Tech. Proc. Eighth Int. TOVS Study Conf.*, Queenstown, New Zealand, IAMAS/ITWG, 395–404.

Smith, W. L., H. M. Woolf, C. M. Hayden, D. Q. Wark, and L. M. McMillin, 1979: The TIROS-N Operational Vertical Sounder. *Bull. Amer. Meteor. Soc.,* **60,** 1177–1187.

Spencer, R. W., J. R. Christy, and N. C. Grody, 1990: Global at-mospheric temperature monitoring with satellite microwave measurements: Method and results. *J. Climate,* **3,** 1111–1128.

Yu, T.-W., and R. D. McPherson, 1984: Global data assimilation experiments with scatterometer winds from Seasat-A. *Mon. Wea. Rev.,* **112,** 368–376.

Zapotocny, T. H., and Coauthors, 2000: A case study of the sen-sitivity of the Eta Data Assimilation System. *Wea. Forecast-ing,* **15,** 603–621.

——, W. P. Menzel, J. P. Nelson III, and J. A. Jung, 2002: An impact study of five remotely sensed and five in situ data types in the Eta Data Assimilation System. *Wea. Forecasting,* **17,** 263–285.

——, ——, J. A. Jung, and J. P. Nelson III, 2005a: A four-season impact study of rawinsonde, GOES, and POES data in the Eta Data Assimilation System. Part I: The total contribution. *Wea. Forecasting,* **20,** 161–177.

——, ——, ——, and ——, 2005b: A four-season impact study of rawinsonde, GOES, and POES data in the Eta Data Assimi-lation System. Part II: Contribution of the components. *Wea. Forecasting,* **20,** 178–198.